



## Unsteady diffusion effects on electrodeposition into a submicron trench

R. CHALUPA, Y. CAO and A.C. WEST\*

Department of Chemical Engineering, Columbia University, New York, NY 10027

(\*author for correspondence, 500 West 120th Street, Room 812, New York, NY 10027,

fax: 212 854 3054, e-mail: acw17@columbia.edu)

Received 6 March 2001; accepted in revised form 9 October 2001

**Key words:** copper electrodeposition simulation, galvanostatic, potentiostatic, submicron features, unsteady diffusion

### Abstract

Electrodeposition of a metal into rectangular cross-section trenches by the application of a current or potential step is investigated via numerical simulations. The feasibility of decoupling of the phenomena occurring on scales of the trench filling time and the species diffusion time is examined. Short time scale events under potentiostatic plating conditions are compared with those events that occur under galvanostatic conditions. Two numerical schemes, the finite volume method (FVM) and the boundary element method (BEM), are used in solving the unsteady diffusion problems. Furthermore, unsteady diffusion with nonlinear reaction rate kinetics on the cathode is considered.

### List of symbols

$c$  local concentration of metal ions or additive species ( $\text{mol m}^{-3}$ )  
 $c_\infty$  bulk concentration ( $\text{mol m}^{-3}$ )  
 $D$  diffusion coefficient ( $\text{m}^2 \text{s}^{-1}$ )  
 $f$  the normal derivative of the concentration ( $-\partial c/\partial n$ )  
 $F$  faradaic constant ( $96\,487 \text{ C mol}^{-1}$ )  
 $h_0$  initial height of trench (m)  
 $i$  local current density ( $\text{A m}^{-2}$ )  
 $i_L$  mass transfer limited average current density ( $\text{A m}^{-2}$ )  
 $i_\infty$  current density assuming uniform concentration equal to bulk value ( $\text{A m}^{-2}$ )  
 $K$  Langmuir constant ( $\text{mol m}^{-3}$ )  
 $k_c$  kinetic constant in nonlinear kinetics ( $\text{mol m}^{-2} \text{s}^{-1}$ )  
 $L$  initial width of trench (m)  
 $L_D$  diffusion boundary layer thickness (m)  
 $n_e$  number of electrons being transferred  
 $n_x$   $x$ -component of the outward normal unit vector (m)  
 $n_y$   $y$ -component of the outward normal unit vector (m)  
 $q$  charge passed to the cathode (C)  
 $q^*$  normal derivative of the fundamental solution ( $-\partial u^*/\partial n$ )  
 $s$  coordinate that follows the cathode surface profile (m)  
 $t$  time (s)  
 $t_F$  ‘observation time’ coordinate (s)

$u^*$  fundamental solution (Green’s function for a point source)  
 $V_m$  molar volume of deposited metal ( $\text{m}^3 \text{mol}^{-1}$ )  
 $x$  horizontal coordinate (m)  
 $\vec{x}$  spatial coordinates of the ‘observation point’  
 $y$  vertical coordinate (m)

### Greek symbols

$\alpha$  parameter in the BEM formulation that takes on values of either 0, 1/2 or 1.  
 $\frac{\partial c}{\partial n}$  normal component of flux ( $\nabla c \cdot \vec{n}$ , where  $\vec{n}$  = outward unit normal vector)  
 $\varepsilon$   $y$ -location at which simulation domain is truncated during a transient-steady hybrid modeling approach (m)  
 $\Gamma$  domain boundary  
 $\eta_S$  cathode surface overpotential (V)  
 $\theta$  fractional surface coverage  
 $\tau_D$  diffusion time inside the trench,  $h_0^2/D$  (s)  
 $\tau_\delta$  diffusion time through diffusion boundary layer,  $L_D^2/D$  (s)  
 $\tau_{\text{fill}}$  filling time for trench, Equation 1 (s)  
 $\vec{\xi}$  spatial coordinates of the ‘source point’

### Subscripts

avg spatially averaged quantity over cathode surface  
 bottom at the bottom centre of the trench  
 cathode integration carried out over cathode surface  
 $\text{Cu}^{2+}$  a property of a cupric ion  
 D corresponding to the diffusion time inside the feature

fill corresponding to the filling time  
 LA a property of a levelling agent  
 SS steady-state value  
 top along the cathode surface outside of the trench

## 1. Introduction

Generally, nonuniformities in current distribution on an electrode are caused by nonuniform reactant concentrations and by spatial variations in the electrical potential difference across the electrode–electrolyte interface [1]. West et al. [1] have shown via a Wagner number analysis that for a typical copper plating bath the charge transfer resistance at the electrode surface far outweighs the ohmic resistance of the electrolyte solution for feature sizes on the order of one micron. In fact, electrical potential fields often have negligible effect on current distribution on length scales smaller than about 10–100  $\mu\text{m}$ . However, the electrical potential fields may be expected to have the dominant effect on the current distributions for length scales larger than approximately 1000  $\mu\text{m}$  at currents well below the limiting values.

For small features (1  $\mu\text{m}$ ), it is the nonuniformity in one or more concentrations near the electrode surface that dictates the current distribution. In the case of an additive-free plating bath in which only the metal cation participates in the cathode reaction, it is the concentration field of that ion that dictates the current distribution on the short length scales. However, in plating baths containing a variety of ‘cathode-active’ additive species, it is often the case that the variations in metal ion concentration are of secondary importance and can be neglected relative to the concentration-field nonuniformities of the additive species [2]. Due to the presence of an excess of a supporting electrolyte, the electrical migration contribution to mass transport of reactants in the solution is negligible. Furthermore, Takahashi and Gross [3] have shown that for submicrometric features (i.e.,  $<10^{-6}$  m), the convective mass transport into the feature can be neglected relative to the diffusive contribution. Convection, however, plays an important role in transporting additives and reactants to a feature mouth.

The quasi-steady state approach for treatment of mass transfer in electrodeposition prevails in the current distribution and shape change literature [2, 4–6]. Under this assumption, the relaxation of the concentration fields inside the liquid electrolyte phase occurs much faster than the deformation of the cathode’s surface due to metallization. Thus, numerical modeling is reduced to solving a steady state diffusion equation and accounting only for the transient behaviour of the cathode’s surface.

The justification for this approach lies in the wide separation of time scales associated with diffusion and with the growth rate of the cathode’s surface. The latter of these time scales is given by:

$$\tau_{\text{fill}} \sim \frac{n_e F}{V_m i_{\text{avg}}} \times \frac{L}{2} \quad (1)$$

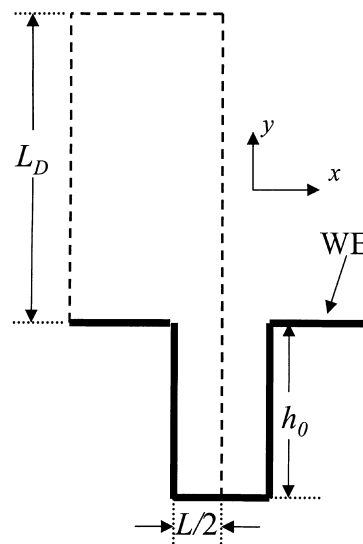


Fig. 1. Rectangular cross section feature and a section of the diffusion layer ( $L_D$  in thickness). WE, working electrode.

The initial cathode geometry we have in mind here is a rectangular cross-section trench. The characteristic length appearing in Equation 1,  $L/2$ , is the half width of such a feature. Figure 1 summarizes the relevant geometric parameters. As Equation 1 shows, the filling time decreases with a decrease in the characteristic size of the feature. The goal of the present work is to examine the validity of the quasi-steady state assumption as the feature size or the agitation of the solution outside of the feature is varied. The effects of the nature of the diffusing species (metal ion or a large additive species) and the type of reaction kinetics on the cathode surface are also examined. Furthermore, the differences in galvanostatic and potentiostatic operation modes are addressed.

## 2. Theory

### 2.1. Diffusion time scales

Two diffusion time scales can be defined in the present problem. First, is the diffusion time of a reactant or additive inside of a trench, given by:

$$\tau_D \sim \frac{1}{D} h_0^2 \quad (2)$$

The second diffusion time scale is related to the diffusion through a concentration boundary layer,  $L_D$  in thickness [7], and is given by:

$$\tau_\delta \sim \frac{1}{D} L_D^2 \quad (3)$$

The relative importance of the two diffusion time scales in comparison with the filling time scale will be discussed.

## 2.2. Potentiostatic and galvanostatic conditions compared

Unless otherwise specified, first order reaction kinetics were assumed on the working electrode [1, 5]:

$$i = cf(\eta_S) = -\left(\frac{i_\infty}{c_\infty}\right)c \quad (4)$$

where  $i_\infty$  is the current density (dependent on the surface overpotential,  $\eta_S$ ) that would be observed if the reactant concentration remained constant everywhere along the working electrode surface. Simulations were carried out in two ways: potentiostatically, where  $i_\infty$  (i.e.  $\eta_S$ ) was kept constant and the resulting average current density,  $i_{\text{avg}}$ , varies with time; and galvanostatically, where  $i_\infty$  (i.e.,  $\eta_S$ ) was adjusted at each time step so as to maintain a constant  $i_{\text{avg}}$ . Comparisons between the two at short times were conducted in such a way that the potentiostatic and galvanostatic simulations converged to the same steady-state value.

## 3. Numerical simulations

### 3.1. Modelling approaches

The separation of time scales allows for a considerable simplification when conducting numerical simulations. Specifically, the ability to ignore unsteady diffusion effects when simulating  $\tau_{\text{fill}}$ -scale events reduces the problem to a Laplace equation which can then be treated simply by a boundary element method (BEM) with no domain integrals present in the formulation [2, 4]. Thus, since only the domain boundary needs to be discretized, this is the approach of choice when dealing with domains that change shape. The  $\tau_D$ -scale events can be easily simulated by numerous methods, including a finite volume method [9] (FVM, present work), a finite difference method [1], or a boundary element method for transient problems (BEM, present work) on a domain with a fixed geometry [8, 10].

An alternative is a one-dimensional simulation (ignore the  $x$ -direction variations in concentration inside the feature [1, 5]) that accounts for both the shape evolution of the cathode due to metallization and captures the unsteady diffusion effects at the cost of overlooking the variations in the transverse direction ( $x$ -direction in Figure 1). A ‘full’ two-dimensional simulation package that does away with the above assumptions and addresses the unsteady diffusion and shape evolution effects in a self-consistent way is a more formidable problem than the above outlined approaches.

### 3.2. Present solution methods

For the simulations carried out on diffusion time scales, the unsteady, two-dimensional diffusion equation,

$$\frac{\partial c}{\partial t} = D\left(\frac{\partial^2 c}{\partial x^2} + \frac{\partial^2 c}{\partial y^2}\right) \quad (5)$$

was solved in one of two ways: via an explicit finite volume method implemented on a uniform, orthogonal grid [9] or via a constant element (in both space and time) BEM [10]. The present BEM is described briefly in the Appendix.

It should be noted that the BEM-based approach to solving Equation 5 can be reduced to a boundary-only formulation for certain initial concentration fields [10]. Thus, the present BEM approach is unsuitable for simulating unsteady diffusion effects on a domain that is changing shape. The major advantage of the BEM lies in the fact that, since only the boundary needs to be discretized, arbitrarily shaped domains are handled with ease. Superior speed of computation as well as high stability of solution that allows for the use of a variable time step are the additional advantages of the BEM compared with the explicit FVM.

The numerical convergence of the FVM was determined by running the simulations with progressively smaller time steps until the results did not show any further variation. Similarly, several node point densities were tried. It was determined that 6 by 8 nodes inside the trench (in the case of  $h_0/L = 4$ ) were sufficient for convergence. The BEM was found to be unconditionally stable with respect to time. Approximately 40 node points were placed per  $h_0$  in the case of BEM. This node point density was maintained over the entire cathode surface and on the domain boundaries near the cathode surface (up to  $2h_0$  above cathode). A more sparse node point density was used further from the cathode (approximately 20 nodes per  $20h_0$ ). The time required for a BEM simulation was a factor of approximately 10 to 50 times less than the FVM.

### 3.3. Metal ion-dictated cathode kinetics

In the case of the FVM approach, boundary conditions were implemented with zero-volume control elements. Zero-flux boundary conditions were imposed at the two symmetry boundaries,  $x = -h_0$  and  $x = L/2$ . First order reaction kinetics were assumed everywhere on the working electrode. Under potentiostatic plating conditions, this translates to the following:

$$D\frac{\partial c}{\partial n} = \frac{i}{2F} = -\frac{i_\infty}{2Fc_\infty}c \quad (6)$$

The value of  $i_\infty$  remains constant during the potentiostatic deposition. Under galvanostatic plating conditions, the following constraint is imposed on Equation 6:

$$i_{\text{avg}} = \frac{\int_{\text{cathode}}^{ids}}{c_\infty} = -\frac{i_\infty(t)}{c_\infty} \frac{\int_{\text{cathode}}^{cds}}{\int_{\text{cathode}}^{ids}} = \text{constant} \quad (7)$$

Thus, in galvanostatic mode, the value of  $i_{\text{avg}}$  is maintained equal to a preset constant by allowing  $i_\infty$  to vary with time. Finally the source boundary condi-

tion,  $c = c_\infty$ , was imposed at the assumed diffusion layer thickness distance of  $L_D$ .

Numerically, the galvanostatic case was treated by an FVM approach only. Galvanostatic cases were implemented by correcting  $i_\infty$  (via a bisection method) at every time step and recalculating the resulting  $i_{\text{avg}}$  until convergence with the set current density occurred. The problem can be made dimensionless, resulting in two dimensionless groups:  $c_\infty V_m$  and  $(i_\infty h_0 / F D c_\infty)$ . The group  $c_\infty V_m$  is set to 0.0018, corresponding to copper deposition from a 0.24 cupric sulfate bath, and the second group may be interpreted as the dimensionless copper plating rate [1, 5].

The charge passed ratio,  $q_{\text{avg}}/q_{\text{avg,D}}$ , appearing in Figure 5 is defined as follows:

$$\frac{q_{\text{avg}}}{q_{\text{avg,D}}} = \frac{\int_0^t i_{\text{avg}} dt}{i_{\text{avg,SS}} \tau_D} \quad (8)$$

where  $i_{\text{avg}}$  is the current density averaged over the cathode surface. Physically, this ratio provides an estimate of the average deposited film thickness normalized by the thickness that is achieved in a time equal to the diffusion time constant.

### 3.4. Levelling agent-dictated cathode kinetics

For the case of a leveling agent-dictated current distribution, boundary conditions on the cathode are given by [2, 5]:

$$D \frac{\partial c}{\partial n} = -k_c \theta \quad (9)$$

where the fractional surface coverage,  $\theta$ , is assumed to follow a Langmuir relationship:

$$\theta = \frac{c}{c + K} \quad (10)$$

The local current density on the cathode surface is given by [5]:

$$i = -i_\infty \left( \frac{1 - \theta}{1 - \theta_\infty} \right) \quad (11)$$

In making the problem nondimensional, two dimensionless groups arise [5]:  $(k_c h_0 / D c_\infty)$  and  $K/c_\infty$ . The value of the former was set to 0.04; the latter was set to 0.02 in all cases. These values provide effective levelling in baseline simulations. In general these values may be expected to be a function of applied potential. However, the spatial variations in these values due to electrical-potential variations are negligible for features of micrometre scale [1]. The nonlinear boundary condition problem was treated via the BEM approach.

## 4. Results and discussion

### 4.1. Separation of time scales

Figure 2 shows the variation of  $\tau_D$  and  $\tau_{\text{fill}}$  with initial feature width,  $L$ . The aspect ratio of the feature,  $h_0/L$ , was set to four. The Nernst boundary layer diffusion times,  $\tau_\delta$ , have also been included in the figure. The two bottom plots (dashed lines) are the diffusion times for two different diffusion coefficients,  $10^{-5} \text{ cm}^2 \text{ s}^{-1}$  and  $10^{-7} \text{ cm}^2 \text{ s}^{-1}$ . The two horizontal plots (dotted lines) appearing at the top of Figure 2 are the diffusion times through a diffusion boundary layer ( $L_D$  in Figure 1). It should be noted that for fixed fluid flow conditions,  $L_D$  changes with the diffusion coefficient ( $L_D \sim D^{1/3}$ ) and thus  $\tau_\delta \sim D^{-1/3}$  [11].  $L_D$  was chosen to be  $35 \mu\text{m}$  for  $D = 10^{-5} \text{ cm}^2 \text{ s}^{-1}$ ; this is about  $7.6 \mu\text{m}$  for  $D = 10^{-7} \text{ cm}^2 \text{ s}^{-1}$ . This corresponds to approximately 200 rotations per minute on a rotating disc electrode, a realistic value for many commercial fountain platers [3]. Finally, the solid line at the top of the Figure represents the  $\tau_{\text{fill}}$  variation with feature size.

Since  $\tau_\delta$  and  $\tau_D$  are much less than  $\tau_{\text{fill}}$  for common values of  $i_{\text{avg}}$  (say,  $10 \text{ mA cm}^{-2}$ , which was used in Figure 2) and for feature sizes ranging from about  $100 \text{ nm}$  to about  $200 \mu\text{m}$ , any deformation of the

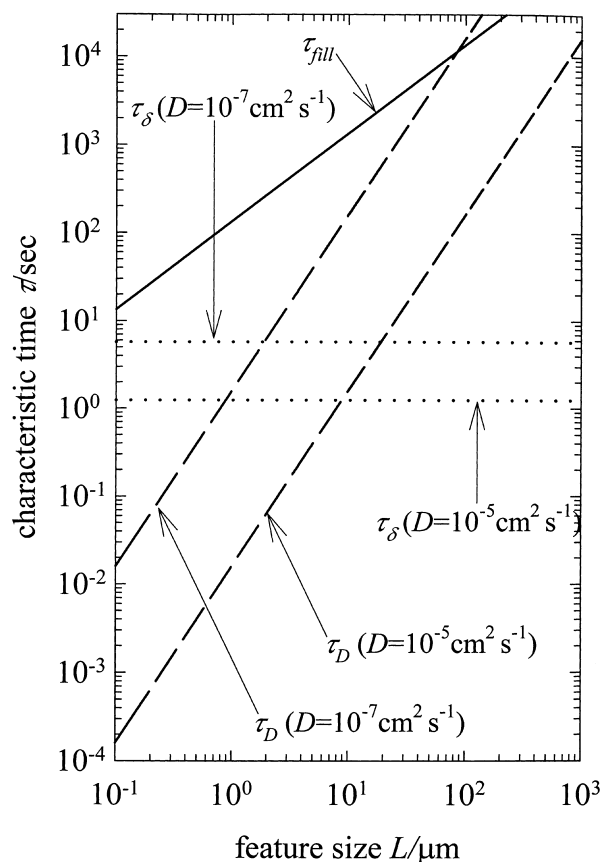


Fig. 2. Variation of characteristic time scales with feature width,  $L$ . Solid line represents  $\tau_{\text{fill}}$ ; dashed lines represent  $\tau_D$  for two different values of the diffusion coefficient; dotted lines represent  $\tau_\delta$  for two different diffusion coefficients.

trench's initial shape due to metallization can be ignored when examining the events occurring on time scales of  $\tau_D$  or  $\tau_\delta$ . This wide separation of time scales allows one to investigate the filling time events under the assumption that the rate of shape deformation of the trench due to metallization on its surfaces is slow compared to the rate of metal ion diffusion in the trench. Thus, in this range of feature sizes, the quasi-steady approach is applicable. Figure 2 shows that below about 100 nm the unsteady diffusion effects (especially for large additive species with relatively small diffusion coefficients) associated with the boundary layer may be important as  $\tau_{\text{fill}}$  decreases to the point where it is comparable with  $\tau_\delta$ .

Figure 3 shows the time dependence of the ratio of local current densities outside the feature and at the bottom of the trench with time under both potentiostatic (solid line) and galvanostatic (dashed line) plating conditions. Results corresponding to four different plating currents are shown. The indicated plating current values have been normalized by the mass transfer limited average current density,  $i_L$ . The local current density ratio shown on the  $y$ -axis is significant since it allows the prediction of void size on the  $\tau_{\text{fill}}$  scale. The potentiostatic results of Figure 3 show that for linear kinetics on the cathode's surface  $i_{\text{bottom}}/i_{\text{top}}$  comes to within a few percent of its steady state value before or near  $t = \tau_D$ . The transient behaviour of the concentration field outside the feature during  $\tau_D < t < \tau_\delta$  has

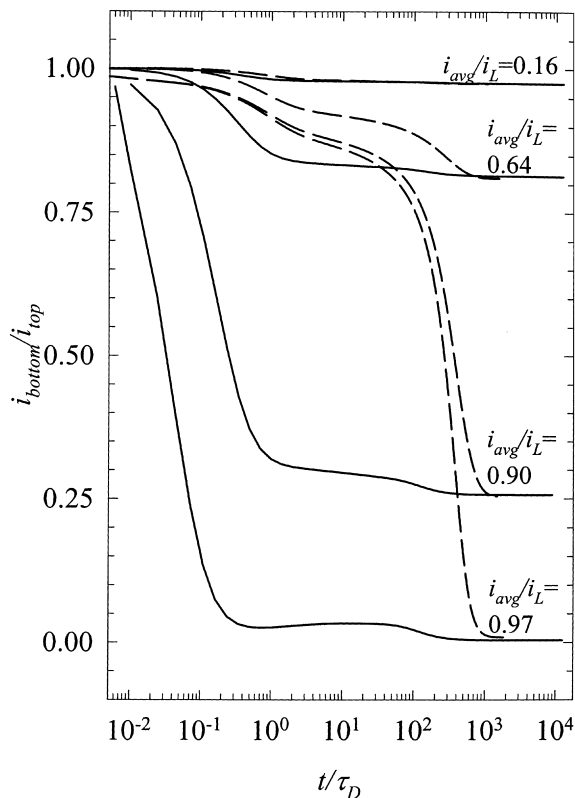


Fig. 3. Behaviour of the ratio of local current densities at the bottom of and outside of the feature in the potentiostatic (solid lines) and galvanostatic (dashed lines) cases. Indicated average currents correspond to steady state values;  $h_0/L = 4$ ,  $L_D/h_0 = 20$ ,  $\tau_\delta/\tau_D = 400$ .

relatively little impact on the current distribution inside the trench. Hence, it is  $\tau_D$  and not  $\tau_\delta$  that should be used as the estimate of when the unsteady diffusion effects on the current distribution inside the feature have subsided. Therefore, it is expected that the quasi-steady state approach will be progressively more valid as the feature size shrinks below 100 nm (see Figure 2) under potentiostatic plating conditions.

#### 4.2. Galvanostatic and potentiostatic conditions compared

The galvanostatic results presented in Figure 3 show a different transient behaviour from the corresponding potentiostatic cases. The bulk of the decay of  $i_{\text{bottom}}/i_{\text{top}}$  to its steady state value occurs during  $\tau_D < t < \tau_\delta$ . The unsteady behaviour of the concentration field inside the diffusion boundary layer has a large impact on the current distribution inside the feature under galvanostatic plating conditions. Thus, according to Figure 2,  $\tau_\delta$ -scale transients can influence feature-filling effects as  $\tau_{\text{fill}}$  becomes comparable to  $\tau_\delta$  below about 100 nm.

Figure 4 shows the variation of the local metal ion concentrations at the bottom of and outside of the feature with time under galvanostatic and potentiostatic plating conditions. The case of  $i_{\text{avg}}/i_L = 0.64$  corresponding to one set of results from Figure 3 was chosen here. Given the dependence of current on metal ion concentration, the current density ratios of Figure 3 are ratios of the local concentrations of metal ions near the electrode surface. Under potentiostatic plating conditions, this ratio reaches its steady state value faster than under galvanostatic conditions, even though local con-

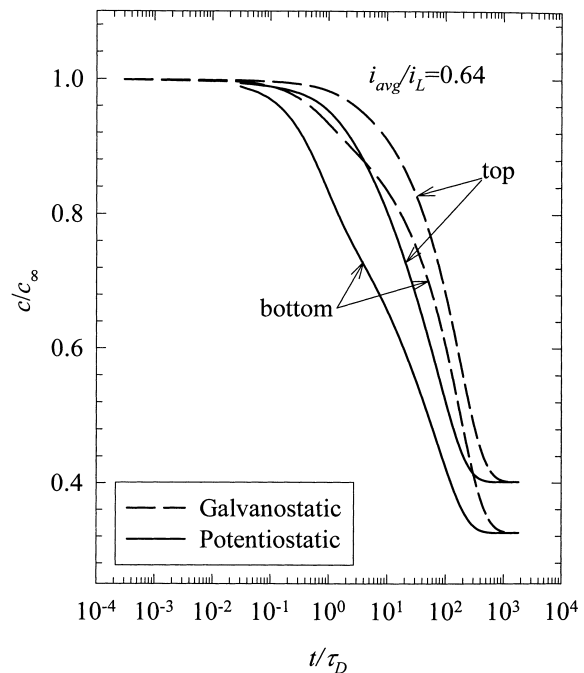


Fig. 4. Behaviour of cupric ion concentration at the bottom of and outside of the feature during potentiostatic (solid lines) and galvanostatic (dashed lines) operations.

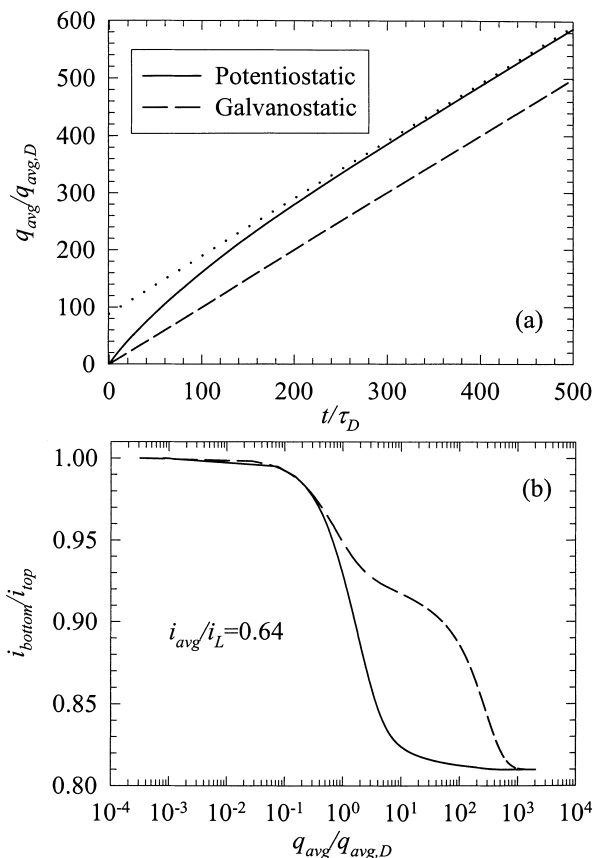


Fig. 5. (a) Behaviour of the average charge passed through the cathode with respect to time in galvanostatic (dashed line) and potentiostatic (solid line) operation modes. (b) Local current densities at the bottom of and outside of the feature with respect to the average charge passed (solid line, potentiostatic; dashed line, galvanostatic). In both plots normalization of charge was done in accordance with Equation 8;  $h_0/L = 4$ ,  $L_D/h_0 = 20$ .

centrations in both cases continue to evolve and reach steady state values at roughly the same time,  $\tau_\delta = 400\tau_D$ .

Figure 5 examines the consequences of the high initial currents observed under potentiostatic plating conditions. Figure 5(a) shows the behaviour of the average charge passed through the cathode as a function of time in both plating modes. The charge ratio being plotted,  $q_{avg}/q_{avg,D}$ , was defined in Equation 8. As expected, the galvanostatic case gives a linear increase in average charge with time. The potentiostatic case, however, shows a rapid and a nonlinear initial (for  $t < \tau_\delta$ ) growth followed by an asymptotic approach to the steady growth rate (dotted line). Figure 5(b) shows current ratio from Figure 3 (for  $i_{avg}/i_L = 0.64$ ) replotted here as a function of the average charge passed. This plot clearly shows that differences exist between potentiostatic and galvanostatic operations even if time is replaced by charge passed.

#### 4.3. Levelling agent against metal ion-dictated current distribution on the cathode

If the current density along the cathode is dictated by reaction kinetics leading to a nonlinear expression such

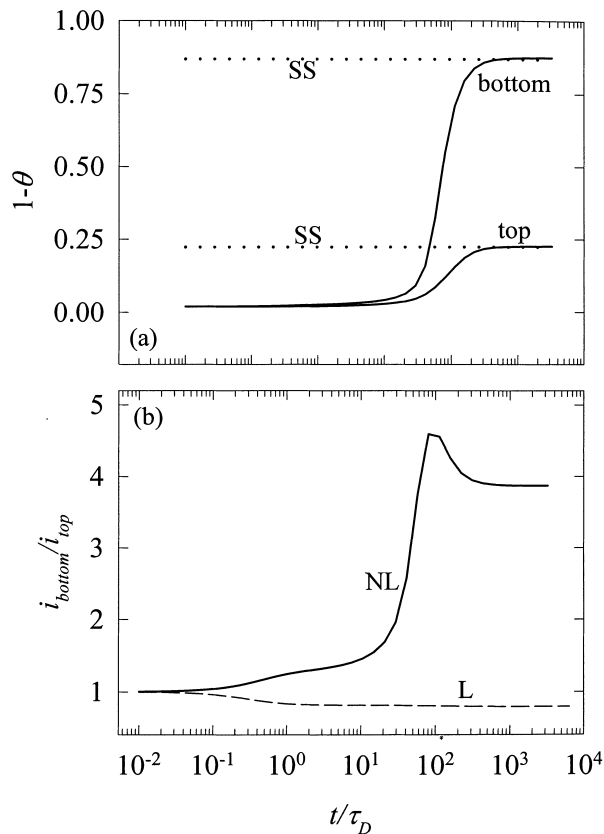


Fig. 6. (a) Behaviour of the fraction of free surface sites at the bottom of and outside of the feature for a  $h_0/L = 4$  trench and  $L_D/h_0 = 20$ . (b) Behaviour of the ratio of local current densities at the bottom of and outside of the feature. Solid line corresponds to the fractional surface coverage results in the top Figure. SS, steady state results; NL, nonlinear boundary condition on the cathode; L, linear boundary condition on the cathode with  $(i_\infty h_0 / FDc_\infty) = 0.08$ .

as Equation 11, the assumption that the current distribution on the cathode is at steady state at  $t = \tau_D$  may start to break down. Figure 6 shows a case where the current distribution inside the feature remains relatively uniform during  $t \leq \tau_D$  but undergoes a drastic variation during  $\tau_D < t \leq \tau_\delta$ . Figure 6(a) shows the variation of the fraction of free surface sites (Equation 10) – the factor that leads to nonuniformities in the current distribution – at the bottom of and outside of the feature with time. Figure 6(b) shows the variation of the resulting local current density ratio. The linear kinetics case, which approaches its steady state value at about  $t = \tau_D$ , has been included as a reference.

The maximum exhibited by the nonlinear kinetics results of Figure 6(b) near  $t \approx 100\tau_D$  can be explained by the behaviour of  $1 - \theta$  in Figure 6(a). Specifically, the fraction of free surface sites at the bottom of the feature undergoes a drastic increase at about  $t \approx 60\tau_D$  (top solid curve in Figure 6(a)) while the fraction outside the feature increases in a relatively sluggish manner to its steady state value. The nonlinear case in Figure 6(b) reaches its steady state at about  $t = \tau_\delta (= 400\tau_D)$ . The results of Figure 6 suggest that the transient effects associated with the diffusion through the concentration

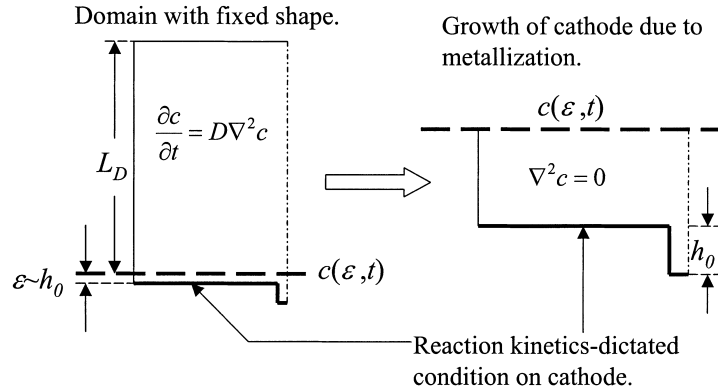


Fig. 7. Domain decoupling procedure. Left: Transient diffusion is solved on the full domain with fixed geometry. Right: Steady diffusion is solved on the truncated domain with an evolving cathode surface.

boundary layer may be important on the  $\tau_{\text{fill}}$ -scale events near or below 100 nm feature sizes (Figure 2). The problem of how to capture those unsteady effects on the shape change simulations ( $\tau_{\text{fill}}$ -scale) in a simple manner thus arises.

#### 4.4. Domain decoupling

Figure 7 suggests a simplified approach applicable when  $L_D \gg h_0$ . One can think of splitting the solution into two parts. First, the transient diffusion problem on the entire, *fixed-shape* domain is addressed (left side of Figure 7). If  $L_D \gg h_0$  is satisfied, the details of the exact shape of the cathode will be unimportant and hence a rectangular domain (i.e., flat cathode) or even a one-dimensional approximation will suffice. Depending on the complexity of the boundary condition on the cathode, the transient diffusion equation may be solved analytically or numerically. Thus, a local concentration at a location slightly above ( $y = \varepsilon$  in the Figure) the cathode is calculated as a function of time,  $c(\varepsilon, t)$ . That concentration can then be used as the ‘counterelectrode’ boundary condition for the steady diffusion problem to be carried out on the truncated domain shown on the right side of Figure 7. This second part of the solution is carried out using a BEM–Laplace equation solver coupled with an algorithm for boundary movement. The value of  $\varepsilon$  is chosen to be large enough so that the thickness of the metal film growing on the cathode will not exceed it. On the other hand, it is advantageous to make  $\varepsilon$  as small as possible so that the unsteady diffusion effects inside the truncated domain remain negligible. In the present work,  $\varepsilon$  was set to  $h_0$ .

Figure 8 shows the results obtained using the ‘domain-decoupling’ outlined in Figure 7. Specifically, the black circles in Figures 8(a) and (b) are for the same case of  $L_D = 20h_0$ . The white circles represent the  $L_D = 80h_0$  case. The dashed lines in both plots were obtained using the BEM for the unsteady diffusion equation and are included for comparison. Shape evolution of the cathode was not accounted for in this Figure so that a direct comparison with the previous results would be possible.

Although it cannot be seen in the Figure 8, the results show the expected discrepancy for  $t \leq \tau_D$ ; the domain decoupling procedure overlooks the transient effects inside the feature. However, for both  $L_D/h_0$  cases, the procedure yields excellent results for  $t > \tau_D$ .

Figure 9 shows the shape evolution results for a 100 nm wide trench. The aspect ratio ( $h_0/L$ ) is 4,

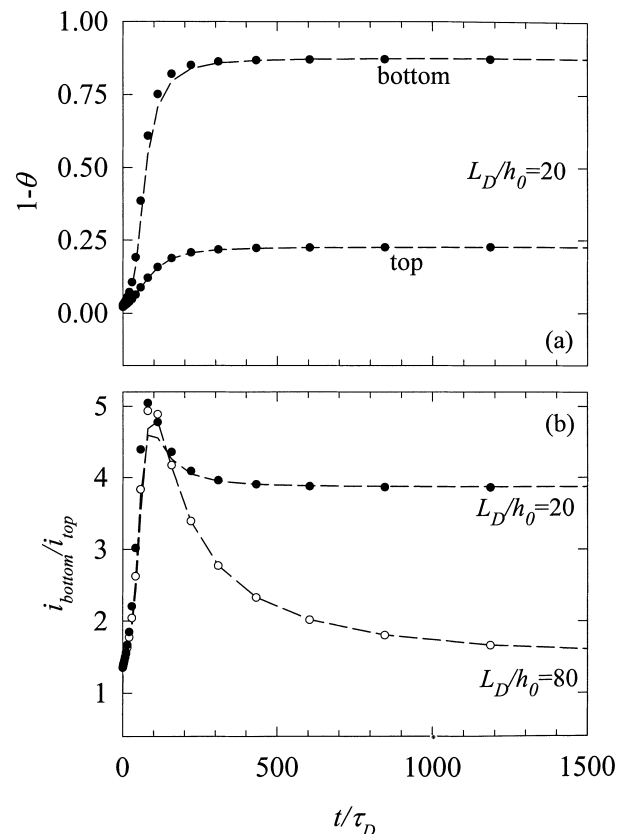


Fig. 8. Comparison of the results obtained using the domain decoupling approach (points) to the results obtained using the unsteady diffusion equation BEM-based solver (dashed lines) performed on a fixed domain.  $h_0/L = 4$ ,  $\varepsilon/h_0 = 1$ . (a) Variation of the local fractional surface coverage at the bottom of and outside of the trench. (b) Behaviour of the ratio of local current densities at the bottom of and outside of the feature.

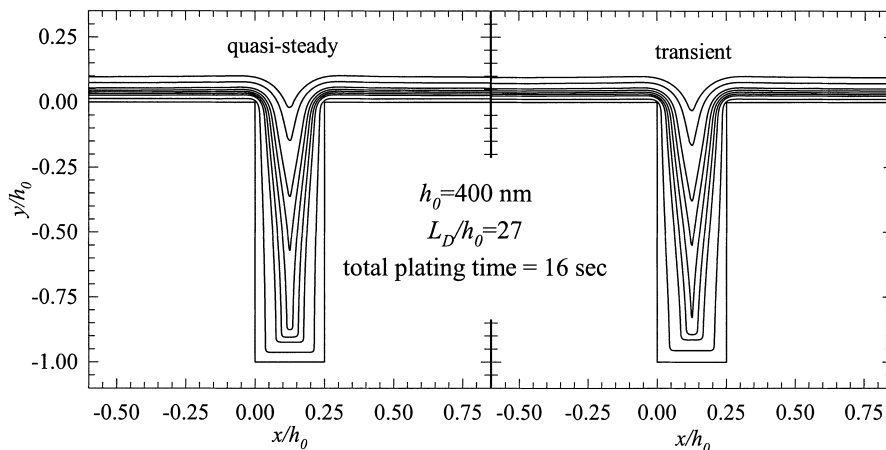


Fig. 9. Shape evolution results obtained in the traditional manner (left side, the quasi-steady state approach) and using the domain-decoupling procedure (right side).

$L_D/h_0 = 27$ ,  $i_{\text{avg}} = 10 \text{ mA cm}^{-2}$ , and  $D_{\text{LA}} = 10^{-7} \text{ cm}^2 \text{ s}^{-1}$ . Results on the left hand side were obtained using the quasi-steady state approach where the steady state value of the current density was used at every intermediate surface profile. Results on the right were obtained using the domain decoupling procedure with  $\varepsilon = h_0$ . Furthermore, it was assumed that the levelling agent kinetic parameters, that is,  $K$  and  $k_c$ , both were potential independent. Hence, the electrodeposition was carried out galvanostatically by maintaining

$$i_{\text{avg}} = - \left[ i_{\infty} \left( \frac{1 - \theta}{1 - \theta_{\infty}} \right) \right]_{\text{avg}} = \frac{-i_{\infty}}{1 - \theta_{\infty}} (1 - \theta)_{\text{avg}}$$

constant. Intermediate profiles of the cathode were plotted more frequently during the time interval where the peak in  $i_{\text{bottom}}/i_{\text{top}}$  of Figure 8(b) occurred. This is where the greatest difference can be seen: the quasi-steady state approach shows relatively more conformal profiles ('weaker levelling') at these intermediate times than the transient model.

## 5. Conclusions

In additive-free plating baths where the current density at the cathode surface depends linearly on the concentration of metal ion in the solution phase adjacent to the electrode surface, transient effects associated with diffusion through the Nernst diffusion layer have relatively negligible effects on the current distribution inside of a submicron feature. The dominant unsteady diffusion effects occur *inside* submicron features but they subside within  $\tau_D$ . Furthermore, since  $\tau_D$  varies with the square of the feature size while the filling time varies linearly with feature size, unsteady diffusion effects will be progressively less important as feature size shrinks. Hence, the quasi-steady state assumption will continue to hold in this case.

However, several factors may lead to a breakdown of the quasi-steady state assumption. If galvanostatic plating is used, unsteady diffusion effects in the boundary layer have a significant influence on the current distribution inside of the feature. These effects subside on time scales of  $\tau_{\delta}$ . When the feature size shrinks to below about 100 nm, feature-filling time may become comparable to  $\tau_{\delta}$  and thus the quasi-steady state approach will start to break down. Furthermore, nonlinearity of the cathode boundary condition can also lead to transient effects in the boundary layer that have a significant influence on the events inside the feature. In this case, a remedy involving a decoupling of diffusion layer transients from the events inside the feature is suggested. This allows for a simplified treatment of unsteady diffusion with an evolving cathode surface.

## Appendix: Boundary element method for the unsteady diffusion equation

The fundamental solution for the unsteady diffusion equation subject to uniform concentration at initial time can be written as [10],

$$\begin{aligned} \alpha(c(\vec{\xi}, t_F) - c_0) &= D \int_0^{t_F} \int_{\Gamma} f(\vec{x}, t) u^*(\vec{\xi}, \vec{x}, t_F, t) d\Gamma(\vec{x}) dt \\ &- D \int_0^{t_F} \int_{\Gamma} (c(\vec{\xi}, t_F) - c_0) q^*(\vec{\xi}, \vec{x}, t_F, t) d\Gamma(\vec{x}) dt \end{aligned} \quad (\text{A1})$$

in which  $f(\vec{x}, t) = -\frac{\partial c(\vec{x}, t)}{\partial n(\vec{x})}$ .

The variable  $\alpha$  in Equation A1 can be 0, 1/2 or 1 depending on whether it is outside the domain, on the boundary or inside the domain. Furthermore, the



fundamental solution,  $u^*$ , and its normal derivative,  $q^*$ , are given by:

$$u^* = \frac{1}{4\pi D(t_F - t)} \exp\left(-\frac{r^2}{4D(t_F - t)}\right) \quad (\text{A2})$$

$$q^* = \frac{d}{8\pi D^2(t_F - t)^2} \exp\left(-\frac{r^2}{4D(t_F - t)}\right) \quad (\text{A3})$$

where  $r = |\vec{\xi} - \vec{x}|$

and  $d = [x(\vec{\xi}) - x(\vec{x})]n_x(\vec{x}) + [y(\vec{\xi}) - y(\vec{x})]n_y(\vec{x})$ .

Collocation method is used to move the point onto the boundary and solve for the unknown concentration or flux. We choose the constant element method for both time and space integration.

### Acknowledgements

This work was supported by the SRC and by the Intel Corporation.

### References

1. A.C. West, C.-C. Cheng and B.C. Baker, *J. Electrochem. Soc.* **145** (1998) 3070.
2. Y. Cao, P. Taephaisitphongse, R. Chalupa and A.C. West, *J. Electrochem. Soc.* **148** (2001) C466.
3. K.M. Takahashi and M.E. Gross, *J. Electrochem. Soc.* **146** (1999) 4499.
4. C. Madore, M. Matlosz and D. Landolt, *J. Electrochem. Soc.* **143** (1996) 3927.
5. A.C. West, *J. Electrochem. Soc.* **147** (2000) 227.
6. J.O. Dukovic, *IBM J. Res. Develop.* **37**(2) (1993) 125.
7. J.S. Newman, *Electrochemical Systems*, 2nd edn. (Prentice Hall, Englewood Hills, NJ, 1991), pp. 400–401.
8. A.C. West and M. Matlosz, *J. Appl. Electrochem.* **24** (1994) 261.
9. J. Deliang Yang, V. Modi and A.C. West, Analysis of mass transfer and fluid flow for electrochemical processes, in B.E. Conway et al. (Eds), 'Modern Aspects of Electrochemistry', Vol. 32, Kluwer Academic/Plenum Publishers, New York, 1999).
10. C.A. Brebbia, J.C.F. Telles and L.C. Wrobel, 'Boundary Element Techniques, Theory and Applications in Engineering' (Springer-Verlag, New York, 1984), pp. 147–152.
11. A.J. Bard and L.R. Faulkner, 'Electrochemical Methods Fundamentals and Applications' (J. Wiley & Sons, New York, 1980), p. 288.